Electronic structures of $Sr_{1-x}La_xRuO_3$

H Nakatsugawa[1], E Iguchi[1], and Y Oohara[2]

[1]*Division of Materials Science and Engineering, Graduate School of Engineering, Yokohama National University, Tokiwadai, Hodogaya-Ku, Yokohama 240-8501, Japan*
[2]*Neutron Scattering Laboratory, Institute for Solid State Physics, University of Tokyo, Shirakata 106-1, Tokai 319-1106, Japan*

Abstract

In order to elucidate a suppression of ferromagnetic interactions in $Sr_{1-x}La_xRuO_3$, electronic structures have been investigated by changing x from 0.0 to 0.5, using an XRD and a neutron diffraction study with a Rietveld analysis and a DV-X alpha computational method. In comparison with magnetic properties in $Sr_{1-x}Ca_xRuO_3$, ferromagnetic interactions in $Sr_{1-x}La_xRuO_3$ are found to be suppressed very rapidly against x. Neither structural distortion nor cation-size disorder can account for such rapid suppression. Instead, this may be attributed to the effect of La - O hybridization created by La substitution for Sr. This hybridization-effect weakens the ferromagnetic order around Ru ions and, as a result, the long-range ferromagnetic states are suppressed even if x is small. The DV-X alpha cluster method was employed to estimate an energy difference between up and down spin density of states in $SrRuO_3$ and $Sr_{0.5}La_{0.5}RuO_3$. This calculation predicts that $Sr_{1-x}La_xRuO_3$ contain La - O hybridization which suppresses ferromagnetic interaction even at small x.

CONTENTS

KEYWORDS

suppression of ferromagnetic states; orthorhombic distortion; cation size disorder; density of states; hybridization

1. INTRODUCTION

Because of the spin-triplet *p*-wave superconductivity in the copper-free layered perovskite Sr_2RuO_4 [1,2], the anomalous magnetic properties and the transport properties in this material and the related ruthenium oxides have attracted much interest. A series of ruthenium oxides $(Sr,Ca)_{n+1}Ru_nO_{3n+1}$ shows rich properties: a ferromagnetic (FM) metal, an antiferromagnetic (AFM) insulator and a superconductor. In particular, a correct understanding of the magnetic properties in these ruthenates is indispensable so as to gain an insight into the emergence of the spin-triplet superconductivity in Sr_2RuO_4.

$SrRuO_3$ and $CaRuO_3$ have nearly cubic and slightly distorted cubic perovskite structure, respectively. Though both the ruthenates exhibit the metallic behavior [3,4], their magnetic properties differ remarkably: $SrRuO_3$ is a FM metal with the Curie temperature T_C=160 K [5,6] whereas $CaRuO_3$ does not show any magnetic anomalies even at very low temperatures. Such a magnetic difference has been mainly ascribed to the ionic sizes of Sr^{2+} (0.144 nm) and Ca^{2+} (0.134 nm), although there must be various reasons. Because of the ionic radius of Sr^{2+} bigger than Ca^{2+}, $CaRuO_3$ is more distorted [5]. In $Sr_{1-x}Ca_xRuO_3$, each RuO_6 octahedron is tilted slightly and rotated around Ca^{2+} substituted for Sr^{2+} to fill the extra space of Sr-shared positions. The calculated band structures also suggest the importance of the structural distortion. In the band structure constructed by Mazin *et al.* [7], the density of states (DOS) in $SrRuO_3$ has a strong peak at Fermi level, stabilizing FM states; while $CaRuO_3$ is on the border of FM states and paramagnetic (PM) states due to the fact that the more distorted structure of $CaRuO_3$ lowers the DOS at Fermi level [7]. In another calculation by Fukunaga *et al.* [8], FM ground states are formed in both the compounds, but the energies obtained in the calculations, especially for $CaRuO_3$, are very sensitive to the calculational parameters employed. It has been also argued that the larger structural distortion in $CaRuO_3$ would result in larger splitting of Ru t_{2g} orbital, leading to stronger AFM interactions [9]. He *et al.* have recently concluded that $CaRuO_3$ is not a classical AFM, but is rather poised at a critical point between FM and PM ground states [10,11].

There are several literatures studying the properties of $Sr_{1-x}Ca_xRuO_3$ perovskites [9-15]. The variation in properties due to the change in x are now basically understood in terms of the change in magnetic ground state as a function of a Ru - O - Ru bond angle [7], but there must be other parameters to consider. The size-disorder of *A*-site atom must be also an important parameter. In the study of the magnetism and the size-disorder effect on the magnetic properties in *4d*-based ruthenate perovskites, the experiments on $Sr_{1-x}La_xRuO_3$ could provide a very useful knowledge. Referring to the ionic radius of La^{3+} (0.136 nm) with the ionic radii of Sr^{2+} and Ca^{2+}, $Sr_{1-x}La_xRuO_3$ is expected to have the orthorhombic distortion and the size-disorder smaller than $Sr_{1-x}Ca_xRuO_3$. In order to investigate the effects due to the orthorhombic distortion and the cation-size disorder, the elucidation of structural lattice parameters in $Sr_{1-x}La_xRuO_3$ as a function of x is indispensable. Furthermore, there is a high possibility that La^{3+} substituted for Sr^{2+} changes the electronic structures on ions and the chemical bond nature. From these points of view, the structural lattice parameters and

the electronic structures in a series of $Sr_{1-x}La_xRuO_3$ perovskites have been investigated in the present study, using the powder X-ray or neutron diffraction methods with a Rietveld analysis and the discrete variational (DV)-X alpha computational method.

2. EXPERIMENTAL DETAILS

Polycrystalline samples of $Sr_{1-x}La_xRuO_3$ (x= 0.0, 0.1, 0.2, 0.3, 0.4, and 0.5) were synthesized by a conventional solid state reaction method. Stoichiometric mixture of powders of $SrCO_3$ (99.99 %), dried La_2O_3 (99.99 %), and dried RuO_2 (99.95 %) were ground and reacted at 1373 K for 24 h in air. This procedure was repeated several times. The samples were reground, pressed into pellets, and heated again at 1573 K for 24 h in air and cooled to room temperature at the rate of 1 K/min in the last procedure. All of the sintered pellets were analyzed at room temperature, using an X-ray diffractometer with step scanning. The powder XRD patterns show a single-phase compound with the *Pnma* type space symmetry (No.62) for every sample. The sample for x=0.5 also was analyzed at room temperature, using a neutron diffraction study. Neutron scattering measurements were carried out on the ISSP triple-axis spectrometer HQR installed at T_{11} experimental port in JRR-3M in JAERI (Tokai). The structural lattice parameters were refined using a Rietveld analysis program, RIETAN-2000 [16].

3. COMPUTATIONAL PROCEDURES

The interpretation of the experimental results obtained here needs the assist of the theoretical calculations. All computations were performed by means of *ab initio* molecular orbital (MO) method using model clusters. The computer code called SCAT [17], which is a modified version of the original DV-X alpha program [18,19], was employed. The exchange and correlation term by Slater with alpha=0.7 was used, and spin polarizations were taken into account in the calculations [20]. Numerical atomic orbitals (NAOs) were used as basis functions. Basis sets were *1s*, *2s*, *2p*, *3s*, *3p*, *3d*, *4s*, *4p*, and *5s* for Sr, *1s*, *2s*, *2p*, *3s*, *3p*, *3d*, *4s*, *4p*, *4d*, *4f*, *5s*, *5p*, *5d*, *6s*, and *6p* for La, *1s*, *2s*, *2p*, *3s*, *3p*, *3d*, *4s*, *4p*, *4d*, *5s*, and *5p* for Ru, and *1s*, *2s*, and *2p* for O. Integrations to obtain energy eigenvalues and eigenfunctions were made numerically. Population analyses were made in the standard Mulliken's manner [21]. The calculation of the electronic structures has been carried out under the assumption that the electronic structures of $[Sr_{16}Ru_3O_{16}]^{12+}$ and $[Sr_8La_8Ru_3O_{16}]^{18.5+}$ clusters are to be representative of those of $SrRuO_3$ (x=0.0) and $Sr_{0.5}La_{0.5}RuO_3$ (x=0.5), respectively. Figure 1 shows the structure of the $[Sr_8La_8Ru_3O_{16}]^{18.5+}$ cluster employed in the present calculation for x=0.5. The model clusters were embedded in Madelung potential generated by approximately 10,000 point charges of formal values. The values were +2, +4, and -2 for Sr, Ru, and O in $SrRuO_3$. In $Sr_{0.5}La_{0.5}RuO_3$, they were +2, +3, +3.5, and -2 for Sr, La, Ru, and O. Convergence of the electrostatic potential with respect to dipole and quadrupole sums [22] was established within an accuracy of 0.1 %.

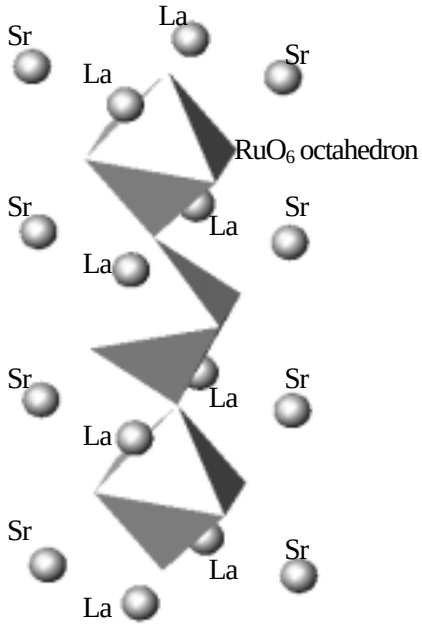

Figure 1. Model cluster used in the DV-X alpha cluster method, i.e., $[Sr_8La_8Ru_3O_{16}]^{18.5+}$ cluster which is employed in the present calculation for $Sr_{0.5}La_{0.5}RuO_3$ (x=0.5).

4. RESULTS AND DISCUSSION

No impurity peak was detected in the present powder XRD or neutron diffraction measurements, and all samples of $Sr_{1-x}La_xRuO_3$ had the $GdFeO_3$ type orthorhombic perovskite structure. Figure 2 shows observed, calculated, and difference intensities in neutron diffraction pattern of $Sr_{0.5}La_{0.5}RuO_3$ (x=0.5). The cubic subcell parameters of $Sr_{1-x}La_xRuO_3$ are shown in Fig.3(a). All three lattice constants, *a*, *b* and *c*, increase with increasing x, although Sr^{2+} (0.144 nm) is replaced with La^{3+} (0.136 nm). There is however an anomaly around x=0.3 in the lattice constant. This must be because electronic structures and magnetic properties change at x=0.3. Furthermore, the Ru - O(1) - Ru and Ru - O(2) - Ru bond angles cross also at x=0.3, as shown in Fig.3(b). The decrease of the Ru - O(1) - Ru bond angle with increasing x suggests the rotation of RuO_6 octahedra around La^{3+} substituted for Sr^{2+} in the similar way to $Sr_{1-x}Ca_xRuO_3$ because of the ionic radius of La^{3+} smaller than Sr^{2+}. The Ru - O - Ru bond angle between RuO_6 octahedra and the Ru - O bond lengths within RuO_6 octahedra change as x increases.

The average net charges evaluated for $[Sr_{16}Ru_3O_{16}]^{12+}$ and $[Sr_8La_8Ru_3O_{16}]^{18.5+}$ clusters at x=0.0 and 0.5 are +2.28*e* and +1.98*e* for Ru, +1.95*e* and +1.97*e* for Sr, and -1.63*e* and -1.43*e* for O, respectively. There must be a small covalent component in the bonding between a cation and an anion. Total DOS and partial DOS of $SrRuO_3$ (x=0.0) and

$Sr_{0.5}La_{0.5}RuO_3$ (x=0.5) are illustrated in Fig.4 together with energy level diagrams. All of the theoretical lines in Fig.4 are the results computed by broadening discrete MO energy eigenvalues, using Gaussian function of 0.5 eV full width at half maximum (FWHM) for easy visualization of the DOS. As shown in Fig.4(a), the filled band located from -10 eV to 0 eV is mainly composed of Ru *4d* and O *2p* orbital at x=0.0. This indicates that the electronic structure around Fermi level consists of Ru *4d* and O *2p* orbital which are hybridized. Figure 4(b) demonstrates the energy levels at x=0.5. The electronic structure around Fermi level consists of Ru *4d*, La *4f*, O *2p* orbital which are also hybridized.

There is an energy difference between up and down spin in Ru *4d* partial DOS which forms FM states. As shown in Fig.5, the energy difference between up and down spin in Ru *4d* partial DOS in $SrRuO_3$ (x=0.0) is larger than that in $Sr_{0.5}La_{0.5}RuO_3$ (x=0.5). This means that FM states are suppressed with increasing x. The unoccupied DOS located above Fermi level is mainly made up of Ru - O and Sr - O hybridization, even though La - O hybridization is included at x=0.5 as shown in Fig.4 (b). The La - O hybridization above Fermi level affects the magnetic local environment around Ru and the local charge state of Ru. Moreover, the local electron densities throughout the Ru - O network and the charge distribution with increasing *x* are likely to fluctuate by this hybridization. Such a fluctuation weakens somewhat the Ru - O hybridization and also the FM interaction between Ru *4d* spins. As a result, FM states in $Sr_{1-x}La_xRuO_3$ are suppressed.

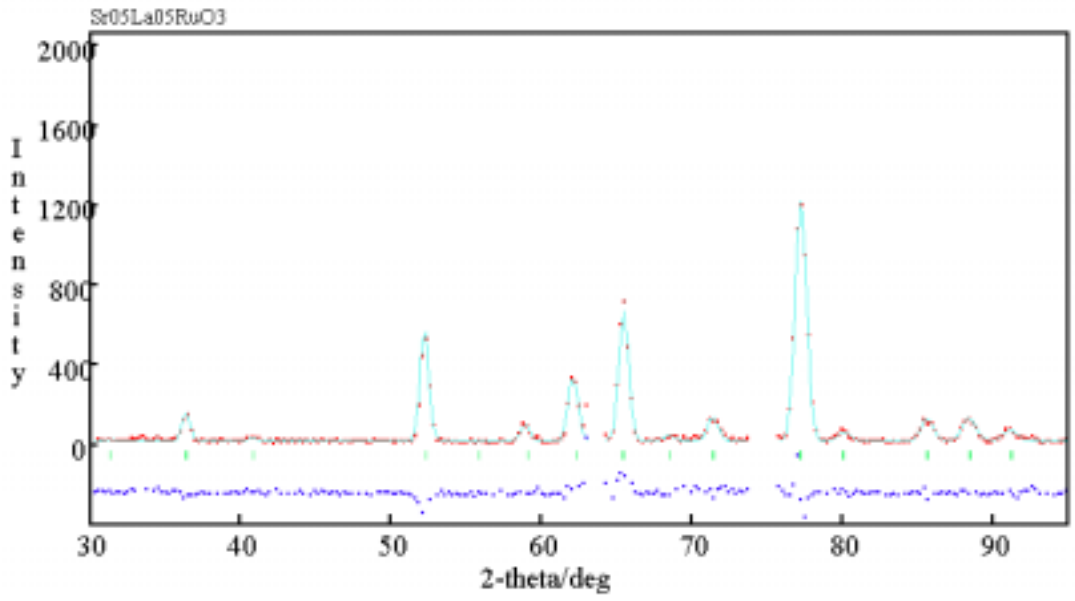

Figure 2. Observed (red dotted line) and calculated (blue line) intensities in powder neutron diffraction of $Sr_{0.5}La_{0.5}RuO_3$ (x=0.5). Tick marks represent the positions of possible Bragg reflections. A blue dotted line at the bottom is the difference between observed and calculated intensities.

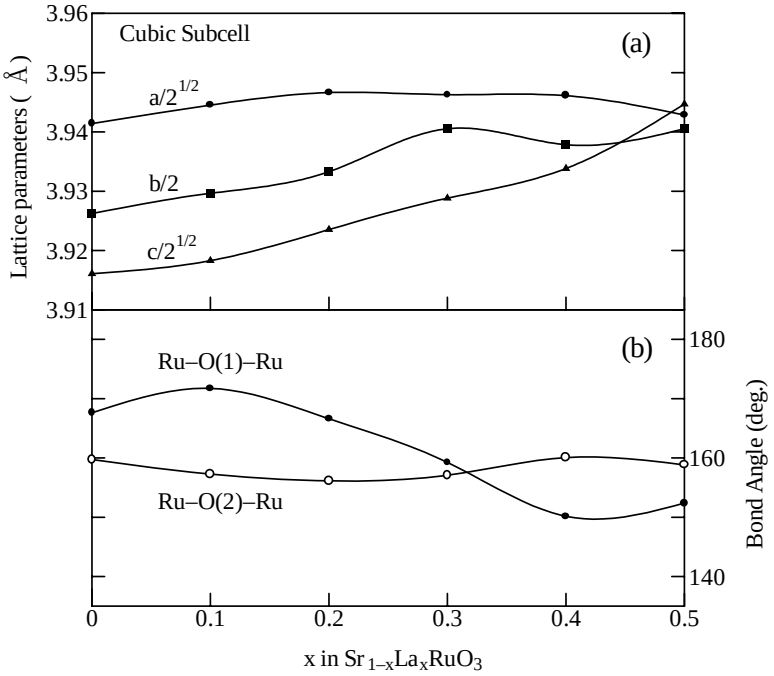

Figure 3. Selected structural data for $Sr_{1-x}La_xRuO_3$. (a) the cubic subcell parameters of $Sr_{1-x}La_xRuO_3$ and (b) the Ru - O(1) - Ru and Ru - O(2) - Ru bond angle. Lines are guides to the eye.

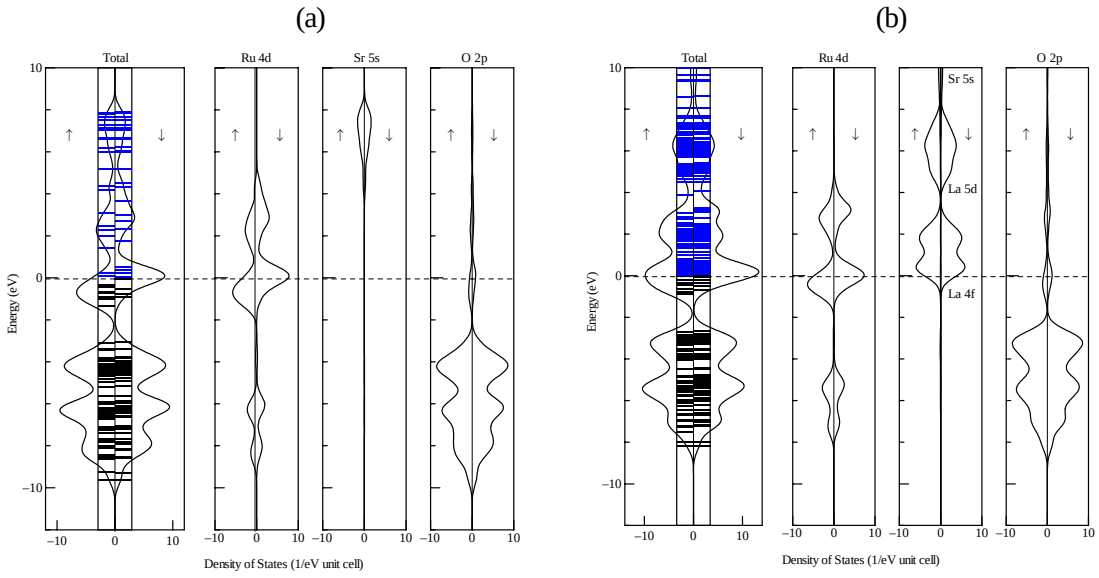

Figure 4. Energy level diagrams and total and partial density of states of (a) $SrRuO_3$ (x=0.0) by $[Sr_{16}Ru_3O_{16}]^{12+}$ cluster and (b) $Sr_{0.5}La_{0.5}RuO_3$ (x=0.5) by $[Sr_8La_8Ru_3O_{16}]^{18.5+}$ cluster.

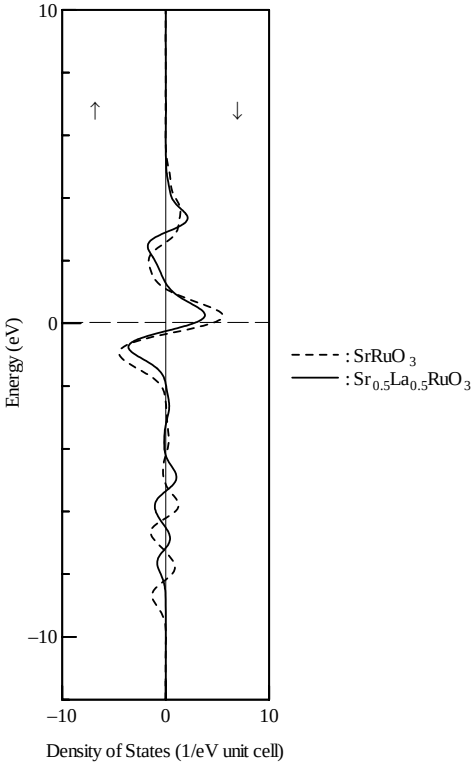

Figure 5. Energy difference between up and down spin density of states, where solid and broken lines indicate that of $SrRuO_3$ (x=0.0) and $Sr_{0.5}La_{0.5}RuO_3$ (x=0.5), respectively.

5. CONCLUSION

The structural lattice parameters and the electronic structures in $Sr_{1-x}La_xRuO_3$ have been investigated using the XRD and the neutron diffraction methods with a Rietveld analysis and the DV-X alpha computational method. The variation of x changes the Ru oxidation so that the Ru - O - Ru bond angle between RuO_6 octahedra and the Ru - O bond lengths within RuO_6 octahedra change as x increases. The ferromagnetism is suppressed very remarkably with increasing x. Since $Sr_{1-x}La_xRuO_3$ contains Ru t_{2g} - O *2p* - Ru t_{2g} interactions, the detailed calculations on the electronic structures in this system are necessary in order to explain the variation of lattice parameters. The energy difference between up and down spin in Ru *4d* partial DOS in $SrRuO_3$ is larger than that in $Sr_{0.5}La_{0.5}RuO_3$. This means that FM states are suppressed with increasing x. In addition, the La - O hybridization above Fermi level affects the magnetic local environment around Ru and the local charge state of Ru. The local electron densities throughout the Ru - O network are likely to fluctuate by the La - O hybridization. Such a fluctuation weakens somewhat the Ru - O hybridization and also the FM interaction between Ru *4d* spins. As a result, FM states in $Sr_{1-x}La_xRuO_3$ are

suppressed.

6. ACKNOWLEDGMENTS

This work was supported by Ogasawara foundation for the promotion of science and engineering and Arai foundation for the promotion of science and engineering.

7. REFERENCES

(1) Y.Maeno, H.Hashimoto, K.Yoshida, S.Nishizaki, T.Fujita, J.B.Bednorz, and F.Lichtenberg, *Nature* (London) **372**, 532 (1994).

(2) K.Ishida, H.Mukuda, Y.Kitaoka, K.Asayama, Z.Q.Mao, Y.Mori, and Y.Maeno, *Nature* (London) **396**, 658 (1998).

(3) H.Kobayashi, M.Nagata, R.Kanno, and Y.Kawamoto, *Mater.Res.Bull.* **29**, 1271 (1994).

(4) G.Gao, S.McCall, M.Shepard J.E.Crow, and R.P.Guertin, *Phys.Rev.* B**56**, 321 (1997).

(5) A.Callaghan, C.W.Moeller, and R.Ward, *Inorg.Chem.* **5**, 1572 (1966).

(6) J.M.Longo, P.M.Raccah, and J.B.Goodenough, *J.Appl.Phys.* **39**, 1327 (1968).

(7) I.Mazin and D.J.Singh, *Phys.Rev.* B**56**, 2556 (1997).

(8) G.Santi and T.Jarlborg, *J.Phys.: Condens. Matter* **9**, 9563 (1997).

(9) F.Fukunaga and N.Tsuda, *J.Phys.Soc.Jpn.* **63**, 3798 (1994).

(10) T.He, Q.Huang, and R.J.Cava, *Phys.Rev*. B**63**, 024402 (2001).

(11) T.He and R.J.Cava, *J.Phys.:Condens.Matter* **13**, 8347 (2001).

(12) K.Yoshimura, T.Imai, T.Kiyama, K.R.Thurber, A.W.Hunt, and K.Kosuge, *Phys.Rev.Lett.* **83**, 4397 (1999).

(13) T.Kiyama, K.Yoshimura, K.Kosuge, H.Michor, and G.Hilscher, *J.Phys.Soc.Jpn.* **67**, 307 (1998).

(14) T.Kiyama, K.Yoshimura, and K.Kosuge, *J.Phys.Soc.Jpn.* **68**, 3372 (1999).

(15) H.Mukuda, K.Ishida, Y.Kitaoka, K.Asayama, R.Kanno, and M.Takano, *Phys.Rev.*B**60**, 12279 (1999).

(16) F.Izumi: *The Rietveld Method* (*Ed.* R.A.Young), *Oxford University Press*, *Oxford*, Chapter 13 (1993)

(17) H.Adachi, M.Tsukada, and C.Satoko, *J.Phys.Soc.Jpn.* **45**, 875 (1978).

(18) F.W.Averill and D.E.Ellis, *J.Chem.Phys.* **59**, 6412 (1973).

(19) D.E.Ellis, H.Adachi, and F.W.Averill, *Surf.Sci.* **58**, 497 (1976).

(20) H.Nakatsugawa and E.Iguchi, *Jpn.J.Appl.Phys.* **39**, 1186 (2000).

(21) R.S.Mulliken, *J.Chem.Phys.* **23**, 1833 (1955).

(22) H.Coker, *J.Phys.Chem.* **87**, 2512 (1983).